Journal of Non-Crystalline Solids xxx (xxxx) xxx–xxx

Contents lists available at ScienceDirect

Journal of Non-Crystalline Solids

journal homepage: www.elsevier.com/locate/jnoncrysol

Temperature dependence of the electrical resistivity and absolute thermoelectric power of amorphous metallic glass $Ni_{33.3}Zr_{66.7}$

B. Smili[a,*], A. Messaoud[b,c,d], W. Bouchelaghem[a], L. Abadlia[a,e], N. Fazel[b], A. Benmoussa[a], I. Kaban[f], F. Gasser[b], J.G. Gasser[b]

[a] Laboratory of Inorganic Materials Chemistry, University Badji Mokhtar of Annaba BP 12, Annaba 23000, Algeria
[b] Laboratoire de Chimie et Physique Approches Multiéchelles des Milieux Complexes LCP-A2MC, Institut de Chimie, Université de Lorraine, 1 boulevard Arago, 57078 Cedex 3 Metz, France
[c] Unité de Recherche Mathématique, Informatique et Physique, Faculté des Sciences de l'Université de Gafsa, Campus Universitaire Sidi Ahmed Zarroug, 2112 Gafsa, Tunisia
[d] Faculté des Sciences de Bizerte, Zarzouna 7021, Tunisia
[e] Laboratoire de Physique de la Matière et du Rayonnement (LPMR), Université Mohamed Chérif Messaadia, B.P. 1553, 41000 Souk-Ahras, Algeria
[f] IFW Dresden, Institute for Complex Materials, Helmholtzstr. 20, 01069 Dresden, Germany

ARTICLE INFO

Keywords:
Metallic glass
Electronic transport properties
Electrical resistivity
Absolute thermoelectric power
Phase transitions
Thermal stability

ABSTRACT

Electron transport properties and thermal stability of $Ni_{33.3}Zr_{66.7}$ metallic glass (MG) have been studied using an original device for simultaneous measurements of electrical resistivity and absolute thermoelectric power (ATP) controlled by a LabView software written by one of us. The electrical resistivity and absolute thermoelectric power were measured simultaneously and very accurately over a temperature range from 25 to 400 °C with a nominal heating rate of 0.5 K min^{-1}. The electronic thermal conductivity was also determined using the Wiedemann–Franz law in the same temperature range. Due to its high efficiency, this technique is more and more used because it is characterized by a high sensitivity to detection of the phase transitions related to electronic transport, which is the aim of this study. Analysis of the temperature dependence of the resistivity and ATP of the $Ni_{33.3}Zr_{66.7}$ glassy ribbons proves the potential of this characterization method to study the thermal behavior of metallic glasses. The crystal structure and the morphology of $Ni_{33.3}Zr_{66.7}$ metallic glass in the as-quenched state and after heat treatments were studied using X-ray diffraction (XRD), and scanning electron microscope (SEM).

1. Introduction

Metallic glasses (MGs) have attracted tremendous attention in the field of materials science and applications over the last few years. Different metallic glasses have been developed with binary and multinary systems [1]. These materials compared to their crystalline counterparts have a series of superior properties such as high mechanical hardness and strength, excellent soft magnetic behavior combined with good corrosion resistance [2–4]. The binary Ni−Zr metallic glass is one of the most studied systems because of its high glass forming ability (GFA) over a wide range of concentrations (30–80 at.% Zr) [5,6], and also for their unusual and unique physical properties, which are very sensitive to any small structural variations [7]. Furthermore, Zr-3d metallic glasses and partially crystalline alloys have a promising profile as interstitial hydrogen hosts because of their high number of tetrahedral sites (hydrogen storage) [7,8]. It is known that these interesting unique properties are directly related to the maintenance of the highly disordered amorphous state (i.e. absence of lattice periodicity and crystalline defects). For this reason, the crystallization of amorphous alloys may reduce the majority of its great advantages especially associated with the amorphous atomic structure.

The operating temperature of MGs is influenced by the glass transition temperature (T_g) and the onset crystallization temperature (T_x), as well as by the temperature dependent behavior, that must be studied to have a clear and precise information about these functional materials and ensure their good exploitation performance. The temperature interval between the glass and crystallization temperatures $\Delta T_x = T_x - T_g$, defines the width of the supercooled liquid region (LSR) which is considered as a basic indicator of the glass forming ability (GFA) and is used for the development of new amorphous alloys

* Corresponding author.
E-mail address: billel.smili@univ-annaba.org (B. Smili).

https://doi.org/10.1016/j.jnoncrysol.2017.11.012
Received 4 September 2017; Received in revised form 30 October 2017; Accepted 9 November 2017

[9]. The thermal behavior of metallic glasses is a topical problem either for fundamental or applied research. The fundamental aspect is directed towards questions relating to the nature of glass, glass transition, and devitrification; as to the applied aspect, it depends on the crystallization and its importance in the development of new generation of amorphous materials having improved functional properties.

Electronic transport properties (i. e. electrical conductivity σ, Seebeck coefficient *S* also called Absolute Thermoelectric Power (ATP) or absolute thermopower, and thermal conductivity k) are among the most sensitive indicators of structural transformations and of their kinetics for all of crystalline, amorphous and liquid conductive materials [10] since these properties are measured with a very high resolution. A variation in the slope is also an indicator of a phase change of matter. Some experimental results obtained via these characterization methods (resistivity and ATP) can be compared to those calculated by various theoretical elaborated models [11,12].

Generally, the electrical conductivity is proportional to the density and to the mobility of the charge carriers. Therefore this characterization technique is more accurate than that of calorimetry (DSC) [13], especially in the case of low heating rate regime $< 0.5\ \mathrm{K\ min^{-1}}$ for long periods of time (non-isothermal mode). From a practical point of view, this new method for simultaneous measurements of electrical resistivity and ATP has the advantage of following the phase variations in resistivity or in thermopower alone or in both at the same time. Thus, the phase transformations can be easily followed during several days (isothermal mode). In addition, the Seebeck coefficient has proved to be an effective means of non-destructive testing of most structural defects on semi-conductors and metallic materials (quality control of materials).

In this work, the amorphous alloy ribbons $Ni_{33.3}Zr_{66.7}$ prepared by the melt spinning technique were studied in detail by electrical resistivity, absolute thermoelectric power and DSC measurements, from room temperature to 400 °C. The amorphous and crystalline structures of the $Ni_{33.3}Zr_{66.7}$ metallic glass have been investigated by X-ray diffraction (XRD) and by scanning electron microscopy (SEM).

2. Experimental procedures

2.1. Sample preparation

Master alloy ingots of $Ni_{33.3}Zr_{66.7}$ (at.%) have been prepared by vacuum arc melting of high purity elements of Ni (99.9%), and Zr (99.9%) under a titanium-gettered Ar atmosphere. The pre-alloyed ingots were re-melted repeatedly in order to assure its compositional homogeneity. Glassy ribbons of 45 μm thickness were prepared by rapid melt solidification technique on a single-roller melt-spinner at a tangential wheel speed of 41 m/s under Ar flow.

2.2. Structural characterization

The phase analysis of the ribbons samples in as-spun and annealed states was carried out by X-ray diffraction (XRD Bruker D8 Advance), at room temperature, using Cuα K radiation ($\lambda = 0.15418$ nm) in the 2θ range (20°–90°), with a step angle of 0.02°. The X-ray diffraction pattern of a pure aluminum sample was used as a standard under the same conditions as the studied amorphous ribbons. The microscopic structure of the ribbons was investigated by means of scanning electron microscope (SEM, JEOL 6300) operating at 25 keV.

2.3. Electrical characterization

The automated measurements of electrical resistivity and absolute thermoelectric power were carried out on an original experimental device working between 300 K and 1600 K. The instrument was designed for the simultaneous measurements of resistivity and ATP using the LabView software for computer data-acquisition [14,15].

The electrical resistivity measurements have been performed with a four-point probe method by means of the passage of a DC current through the two ends of the ribbon (sample), in a circuit containing a standard resistance R_{stand} in series with the sample to be measured. The electrical resistivity of the sample ρ_{samp} is given as:

$$\rho_{samp} = \frac{U_{samp}}{U_{stand}} \times \frac{R_{samp}}{C} \quad (1)$$

where U_{samp} is the voltage drop across the sample, U_{stand} is the voltage drop across the standard resistance, and C is a sample constant characterizing its length (L) and cross-section (S)l. The resolution of the electrical resistivity is better than 0.02%. The standard deviation determined by repeating a large number of measurements at room temperature is lower than 0.05%. Thus, we have an extremely high accuracy on small changes of resistivity and of the slope of the resistivity. There is also a systematic error on all measurements due to the inaccuracy of the determination of the geometry of the sample. We estimated it to be lower than 2% since we measured many times the length, the thickness and the width of the ribbons with a high-resolution micrometer. Temperature measurements are within 1 °C since we recalibrated the emf versus T law. It is necessary to remember that the systematic error on the geometry does not affect the temperature at which the change of the resistivity or of its slope occurs. The absolute thermoelectric power (also called absolute thermopower or absolute Seebeck coefficient) is measured by the small temperature gradient method (differential method), in which ΔT varies symmetrically between − 2 °C and + 2 °C. The Seebeck coefficient of the sample S_{samp} is calculated using the formula described by A. Bath [16]:

$$S_{samp} = \frac{S_{AB}}{P - 1} + S_A \quad (2)$$

where S_{AB} is the Seebeck coefficient of the thermocouple AB (positive leg: chromel/negative leg: alumel), S_A is the Seebeck coefficient of the positive element A (chromel (K) and nicrosil (N) in our case), and *P* is the slope that manages the variations in the voltages ratio $\Delta V_{24}/\Delta V_{13}$. ΔV_{24} is the voltages between alumel-sample-alumel and ΔV_{13} is that between chromel-sample-chromel.

The measurement system is made up of two alumina flat parts with two holes, designed and sintered in the laboratory, ensuring the connection between the thermocouple junctions and the sample measuring points, and holding the sample in a stainless steel sample holder. It enables measurement of different shapes of materials (ribbons, wires, rods …). Four N or K-type thermocouples (T_{ref}, T_{mod}, T_{ext1}, T_{ext2}) calibrated with pure platinum and using the absolute thermoelectric power values of Roberts et al. [17], were used to control the temperature on the four measuring points in contact and around the sample (ribbon). An auxiliary thermocoax heater is used to create a variable with time temperature gradient at both ends of the sample during the ATP measurements. All voltages were measured on each specific channel of scanner card in a Keithley 2000 multimeter with an accuracy better than 0.01%. All electrical wires of thermocouples are assembled in a multi holes ceramic insulating tube of 1 m length, in order to isolate and protect the electrodes and guarantee the mechanical rigidity of the measurement system (auxiliary furnace part). After making the contact of the thermocouples on the two sides of the ribbon (measuring point), the sample holder is fixed inside a quartz tube of 60 mm diameter connected to a vacuum system and Ar pure gas supply. The tube is placed in the center of a horizontal cylindrical furnace equipped with an external control thermocouple connected to a PID temperature controller JUMO dTRON 300, which provides a resolution of temperature of the furnace better than ± 0.1 K. For ATP measurements it is recommended to use a lower heating rates (< 1 °C/min), in order to give a time necessary at each loops (between 4 and 10 min) to ensure high measurement accuracy. In the present work, ATP is determined with a resolution of 0.03 $\mu V\ K^{-1}$ and an accuracy of ± 0.3 $\mu V\ K^{-1}$.The comparison with the standard element made of a very pure

thermoelectric copper wire is at $< 0.1\ \mu V\ K^{-1}$ from the Roberts [17] standard value. In order to avoid the thermoelectric parasitic effects during the resistivity measurement, a new generation of current relays (USB ROPTO 16 from "Digimétrie" company) has been used to establish, cut and invert the current in the sample. A series of the electrical resistivity measurements have been carried out for a ribbon at room temperature with various current ranges (from 10 mA to 200 mA) in order to choose an appropriate value of DC current (40 mA in present work)required to reduce the effect of Joule heating to a negligible value. It has to be noted that in this study, several hardware components of the measuring system such as type thermocouple, sample fixation system, ceramic insulator, auxiliary heater and its self-controlling, current reverser system, and even the data-acquisition program have been developed and improved considerably compared to the measuring device system used previously by Abadlia et al. [18].

It is well known that the sample geometry, difficult to evaluate with precision, is an important parameter for electrical resistivity measurements. Most noteworthy, the knowledge of the most accurate resistivity at room temperature requires extremely precise measurement of the geometrical constant. In practice, we used a specific measurement configuration (PVC blocks) installed inside an isothermal parallelepiped box, containing a special sample holder assuring a very precise dimension of the sample. In order to reduce the error over the sample constant, the sample length is measured several times under a stable and homogeneous temperature. A section of a long ribbon has been measured in a repeated way (at least 20 measurements) with a micropalmer of very high degree of accuracy and precision (resolution of $\approx 1\ \mu m$). The voltages required for resistivity and temperature measurements are taken by the thermocouples placed at the selected locations where the terminals of Keithley 2000 are connected. Generally, this measurement procedure takes over one week and allows resistivity values to be recovered over a linear range between 20 °C and 45 °C. For $Ni_{33.3}Zr_{66.7}$ ribbon, this calibration was conducted without constraints and the obtained measurements are of high accuracy. The overall error on the geometric constant $C = \int_0^L dl/s(l)$ is estimated to be between 1 and 2%.

2.4. DSC experiments

In order to obtain more information on the thermal properties of the studied metallic glass, continuous heating DSC measurements of the ribbon samples were performed using a differential scanning calorimeter (NETZSCH DSC 404) under the protection of high-purity Ar atmosphere at a heating rate of $0.5\ K\ min^{-1}$. The characteristic temperatures (T_x, T_g, and T_p) were determined with a standard error of 0.3 °C.

3. Results and discussion

3.1. Phase change phenomena at low-rate heating

3.1.1. Electrical resistivity measurements

As shown in Fig. 1, the value of electrical resistivity (ρ) of $Ni_{33.3}Zr_{66.7}$ metallic glass measured at room temperature is equal to 180.13 μΩ cm. This high resistivity value is mainly related to the low mean free path of the electrons resulting from the high atomic disorder in metallic glasses. The latter inherited directly from the liquid state generates very interesting physical properties [19]. The room-temperature electrical resistivity of the majority of metallic glasses based on transition metals commonly varies in the range of 50–250 μΩ cm [20]. According to the geometric constant accuracy of the studied sample, our room-temperature resistivity value is in good agreement with those of other similar alloys published elsewhere [21–23]. The temperature dependence of electrical resistivity of the $Ni_xZr_{(x-1)}$ metallic glasses has been reported to show the highest value at the $Ni_{50}Zr_{50}$ composition, which corresponds to the lowest thermopower value [24].

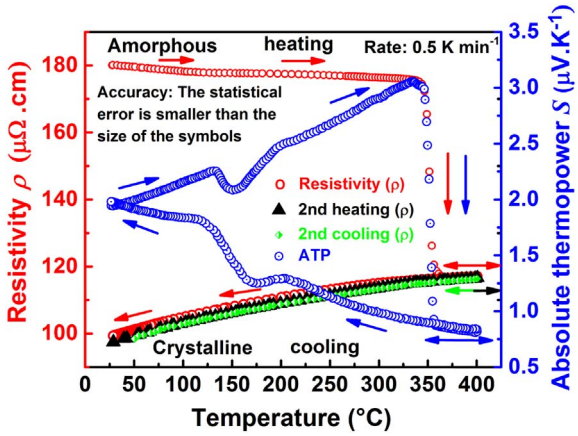

Fig. 1. Measurements of the electrical resistivity (left scale) and ATP (right scale) for the $Ni_{33.3}Zr_{66.7}$ glassy alloy as a function of temperature at a heating rate of $0.5\ K\ min^{-1}$. We can observe the temperature dependence of electrical resistivity for the $Ni_{33.3}Zr_{66.7}$ melt-spun ribbons measured in several successive heating-cooling cycles. The statistical error is very lower than the size of the symbols (≤ 0.05%). The systematic error, which is the same at all temperatures, is of the order of the size of the symbols (≤ 2%), thus does not affect the observation of phase transitions.

Upon the first temperature rise (heating), the electrical resistivity decreases almost linearly up to 330 °C with a negative temperature coefficient of resistivity (TCR) equal to $-1.17 \times 10^{-10}\ \Omega\ m\ K^{-1}$, which is in good agreement with the Mooij correlation [25]. This negative TCR can be interpreted in the frame of the extended Ziman theory [26]. It is well known that the electrical resistivity depends on the number of charge carriers and their mobility at the Fermi energy E_F. Accordingly, the negative temperature coefficient of the resistivity of the $Ni_{33.3}Zr_{66.7}$ metallic glass can be explained by the decreasing intensity of the structure factor $S(Q)$ upon increasing temperature near the Fermi wave vector [27].

The mobility of the charge carriers is expressed in Faber Ziman [28] formula as an integral from zero to $2k_F$ of the product of the structure factor times the form factor squared (or t matrix squared). In this publication, the authors refer to all earlier improvements of the formalism. A change of one of these functions has an important effect on the resistivity. So the resistivity change characterizing the recrystallization of the amorphous alloy corresponds to an important change of the structure factor as can be seen on synchrotron measurements [27]. A more subtle transition is that occurring at the Curie point. It has been experimentally observed on many metals like pure nickel [18] or amorphous alloy like $Fe_{86}Cr_6P_6C_2$ presented at the last LAM'16 conference in Bonn (Germany) by some of us and also in crystalline state [29]. In extended Faber-Ziman formula, the Curie point induces a change in the scattering i.e. in the squared t matrix. Experimentally, the Curie point corresponds to a change of the resistivity temperature coefficient in all the papers cited above.

In the temperature range of 335–360 °C, the resistivity decreases much more rapidly and shows a sharp decline as shown in Fig. 1. This sudden drop indicates a first order phase transformation from amorphous to crystalline structure. Upon further heating from 360 °C, the resistivity begins to increase more slowly with a positive TCR and reaches the value of 117.13 μΩ cm at 400 °C. At this stage, the amorphous ribbon is totally crystallized. The change in slope of the resistivity versus temperature (from negative to positive TCR) after the complete crystallization of the glassy sample (360 °C) can only be explained in the context of the known conductor's ohmic behavior.

The zoomed part of resistivity curve (176–180 μΩ cm area) presented in Fig. 2 shows clearly a change of slope at 120 °C. While above 120 °C, a less pronounced change in slope is observed. This change reflects the phase transition temperature (T_{PT}) which by analogy with identical behaviors of metals, amorphous and crystalline alloys can

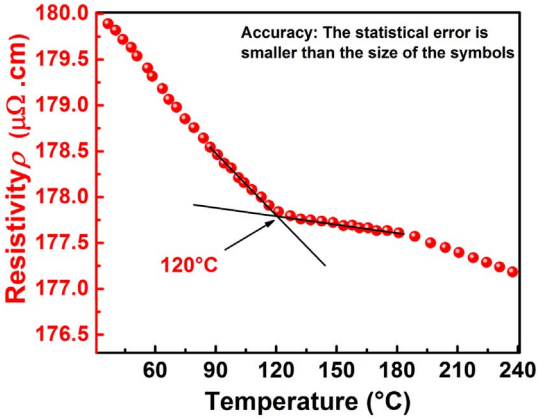

Fig. 2. Expanded scale for electrical resistivity as function of temperature between 40 °C and 240 °C for the $Ni_{33,3}Zr_{66,7}$ amorphous ribbon at heating rate of 0.5 K min^{-1}.The plotted straight lines are a guide to the eyes to determine accurately the temperature of the phase transition.

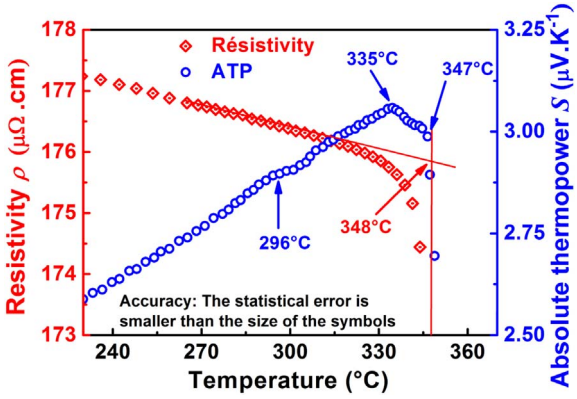

Fig. 3. Expanded scale for measurements of the electrical resistivity (left scale) and ATP (right scale) for the $Ni_{33.3}Zr_{66.7}$ MG as function of temperature at heating rate of 0.5 K min^{-1}.The plotted straight lines are a guide to the eyes to determine accurately the temperature at which a transition begins to occur.

reasonably be considered as a change from a ferro to paramagnetic behavior at the Curie point since Shirakawa et al. [30] reported a concentration dependence of the Curie temperature of TM-Zr alloys. The same phenomenon has been observed in other metallic glasses studied previously [13,27]. Generally, the Curie point is clearly detectable by the resistivity and magnetic susceptibility measurements but goes unnoticed by X-ray diffraction studies as a function of temperature. In resistivity curves, we did not find any other change of slope. We conclude that 120 °C is the Curie temperature of the alloy, but this needs to be confirmed by magnetic susceptibility measurements.

When the temperature decreases (first cooling up to 25 °C), the electrical resistivity of the crystallized $Ni_{33.3}Zr_{66.7}$ ribbon (i.e. heated to 400 °C) varies linearly with a positive temperature coefficient over the whole temperature range. It should be noted that the electrical resistivity value of the crystallized alloy loses 37% of its initial value in the amorphous state (glass), which stabilized at 99.31 μΩ cm.

The variation in electrical resistivity during the crystallization process of metallic glasses is governed at high temperatures by the crystal nucleation and crystal growth, mainly related to the atomic diffusion [31]. Accordingly, the modification of the arrangement of atoms aggregates caused by the appearance of the crystal grains in the residual matrix has a great influence on the atomic and electronic structure of the metallic glasses, which leads to the sudden drop in the value of the electrical resistivity upon crystallization [32]. Similar results have been reported in the works [33,34]. Due to the high resemblance of the electron transport properties [24] between amorphous metals and liquid metals according to the large disorder in atomic structures, the Ziman theory [35] developed especially for liquid metals may also be applied in the analysis of the results of electronic transport properties of amorphous metal alloys. It can eventually be used for crystalline alloys but only at higher temperature.

3.1.2. *Thermoelectric power measurements*

It can be seen from Fig. 1 that the absolute thermoelectric power (i.e. the logarithmic derivative of the resistivity as a function of energy) of $Ni_{33.3}Zr_{66.7}$ metallic glass measured at room temperature is positive and equals to $S = 1.95\ \mu V\ K^{-1}$. This value is slightly lower than those cited in the literature [24,36,37]. This positive ATP value, also reported by Pekala and Oleszak [38], is related to the room temperature resistivity value higher than 150 μΩ cm. The ATP becomes negative when the electrical resistivity falls below 150 μΩ cm [39]. Kaban et al. [27] explained the positive thermopower and the negative temperature coefficient of resistivity using the structure factor $S(Q)$ measurements in terms of the position of the main peak $2k_F$ on the increasing or decreasing side of the structure factor by crystallization of a Ni-Pd-P metallic glass. Hence, structural changes upon heating of a metallic glass lead to a significant modification of the electronic transport properties.

Upon heating, the absolute thermoelectric power increases continuously and almost linearly in the amorphous phase proportionally to the temperature with a positive temperature coefficient up to the first change in the slope corresponding to the glass transition temperature T_g = 296 °C as shown in Fig. 3. This indicates an inherent difference related to the electron transport between the glassy state and the supercooled liquid state. The glass transition temperature (T_g) detected via the variation of the Seebeck coefficient slope is reported for the first time by Peckala et al. [40]. The high-accuracy of our ATP measurements allowed us to detect the glass transition temperature, which in very good agreement with DSC measurements.

Thereafter, the ATP increases continuously up to 335 °C and shows a slight decrease in the interval of 335–347 °C (see Fig. 3). Then it follows an abrupt and sizable decline at T_x = 347 °C similar to that of the resistivity, and giving the lowest value of $S = 0.86\ \mu V\ K^{-1}$ corresponding to the end of the crystallization process. The crystallization onset is observed with ATP and resistivity practically at the same temperature. By further heating above 353 ° Cup to about 400 °C, the ATP decreases slightly with temperature (Fig. 1). Afterward, at cooling, the ATP increases quasi-linearly down to room temperature. Finally, the absolute thermoelectric power of the crystallized ribbon remains positive and reaches a value ($S = 1.94\ \mu V\ K^{-1}$) very close to that of the as-spun (unheated) ribbon.

During the thermoelectric power measurements, a concave bump with a minimum centered at about 155 °C reproducible by heating and cooling, is observed in the temperature range from 125 °C to 200 °C as shown in Fig. 1.This effect does not exist in resistivity measurements. It is thought that this abnormal decrease can be interpreted, either as a physical behavior characteristic of the studied alloy or as a phenomenon related to the thermocouples used (the thermocouples are directly involved in the characterization of the ATP). For that reason, an in-depth study was carried out in order to explain the causes of this abnormal behavior by first focusing on the type of thermocouple. The ATP measurements of $Ni_{33.3}Zr_{66.7}$ metallic glass shown in Fig. 4, in which the chromel-alumel couple (K-type) was replaced by nicrosil-nisil (N-type), have revealed the disappearance of this bump. Hence, the probable relation of this bump with the type of thermocouple used was confirmed by realizing parallel ATP measurements with both types K and N thermocouples on a pure copper sample (ribbon). The results obtained are compared in Fig. 5, with those of Roberts [41], which indicate the presence of the bump with type K thermocouple only and its disappearance with type N thermocouple. In order to check the accuracy of the measuring apparatus, we plot in the inset of Fig. 5 the

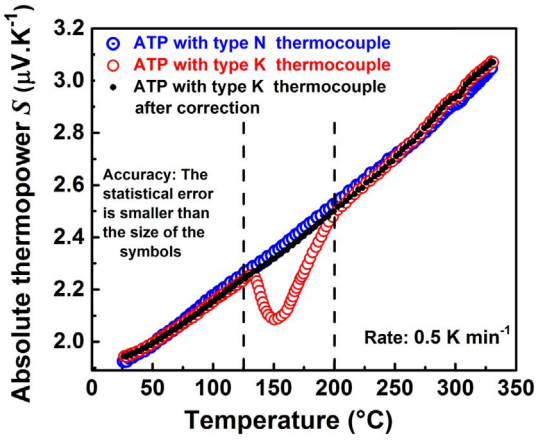

Fig. 4. Measurements of ATP using N thermocouple and K thermocouple (before and after correction) for $Ni_{33.3}Zr_{66.7}$ metallic glass as function of temperature at heating rate of 0.5 K min^{-1}.Vertical lines indicate the temperature region between which the scale of thermoelectric power of K thermocouple is not correct.

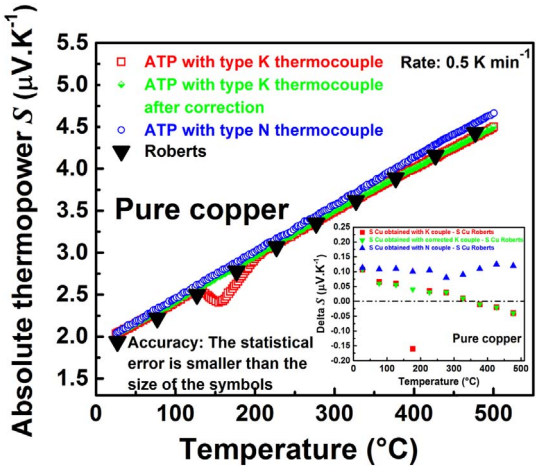

Fig. 5. Thermoelectric power measurements for pure copper as a function of temperature at heating rate of 0.5 K min^{-1}using N thermocouple, K thermocouple before and after application of the new ATP correction formula. The inset shows the difference of ATP between this work and Roberts [41].

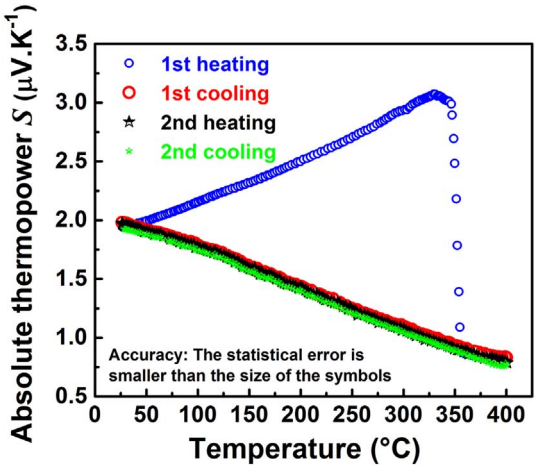

Fig. 6. Temperature dependences of absolute thermoelectric power for the $Ni_{33.3}Zr_{66.7}$ glassy alloys measured in several heating-cooling cycles after the application of the new ATP correction formula.

difference between the thermopower of Roberts and our one as a function of temperature with different thermocouple types. The difference between Roberts values (standard of thermoelectric power) and ours is smaller than 0.10 μV K^{-1} and 0.12 μV K^{-1} when using the type K and type N thermocouple respectively (except at 173 °C), which can be considered as highly accurate measurements.

After a thorough study of the evolution of the thermoelectric power of the chromel/alumel pair, it appears that the problem of this bump is related to the gaussian contribution to the polynomial fit for the chromel/alumel pair obtained from the NIST's thermocouple tables in ASTM book. We measured ATP of an alumel wire by using N-type thermocouple. The measured ATP of alumel is different from that deduced from the ASTM functions. This means that the two alumel wires that we bought are both different from that used by the NIST. It was possible to establish a new correction formula of ATP for alumel and also for the chromel-alumel thermocouple found commercially. Based on the above results, the corrected formula is given by the following expression:

$$S_X = \frac{S_{Cr-Al}}{P-1} + S_{Cr} \tag{3}$$

S_{Cr} and $S_{Cr\text{-}Al}$ are the values that we have determined. Thus, using this formula, the measurements already made have been corrected by the addition of a new Gaussian function whose effect concerns only the temperature area of the bump relative to the thermopower polynomials of the chromel/alumel delivered by the NIST. Therefore, we can confirm that this phenomenon is far from any structural interpretation and is oriented towards the type of K thermocouple.

The curves of the second heating/cooling cycles of electrical resistivity (ρ) and thermoelectric power (S) shown in Fig. 1 and Fig. 6 respectively are almost superimposed and without any inflection. Both resistivity and ATP curves remain perfectly on the same line of the first cooling with a slightly positive temperature coefficient for the electrical resistivity TCR and a linear dependence of a negative temperature coefficient for the absolute thermoelectric power over a wide range of temperatures. We can, therefore, conclude that these reproducible curves confirm the high thermal and structural stability of this alloy after its full crystallization. It should be noted that the ATP value of the crystallized sample after the 2nd cooling up to room temperature, is at 2 hundredths of μV K^{-1} (S = 1.93 μV K^{-1}) compared to the thermopower of the glassy sample (unheated ribbon) at room temperature (S = 1.95 μV K^{-1}).

3.1.3. Deduced thermal conductivity

It is well known that charge transport in materials is mainly governed by the electron displacement, while heat transport occurs through a joint contribution divided between electrons and phonons. Generally, the thermal conductivity of metallic glasses can be defined as the sum of the electronic contributions (k_{el}), and the phonon contributions (k_{ph}) as:

$$k_{total} = k_{el} + k_{ph} \tag{4}$$

However, in most metals, the electronic contribution, k_{el}, to the total thermal conductivity is very larger compared to the low phonon contribution, k_{ph}, which may be neglected [42].

In order to get more information about the electronic-transport properties of $Ni_{33.3}Zr_{66.7}$ metallic glass, the electronic thermal conductivity, k_{el}, generally related to the electrical resistivity and to the thermopower, can, therefore, be calculated based on the Wiedemann-Franz (W−F) law [43]:

$$k_{el} = \frac{(L_0 - S^2)T_k}{\rho} \approx \frac{L_0 T_k}{\rho} \tag{5}$$

Where L_0 is the Sommerfeld value of the Lorenz number ($Lo = 2.45 \times 10^{-8}$ W Ω K^{-2}), and ρ is the electrical resistivity. The simplified expression of Eq.(5), is called the Wiedemann–Franz (W−F) law. It can be used without problems if the Seebeck coefficient is not

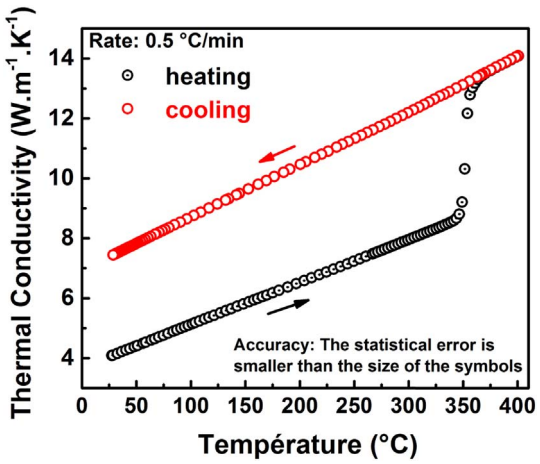

Fig. 7. The temperature dependences of the electronic thermal conductivity for the $Ni_{33.3}Zr_{66.7}$ amorphous ribbon at a heating rate of 0.5 K min^{-1}.

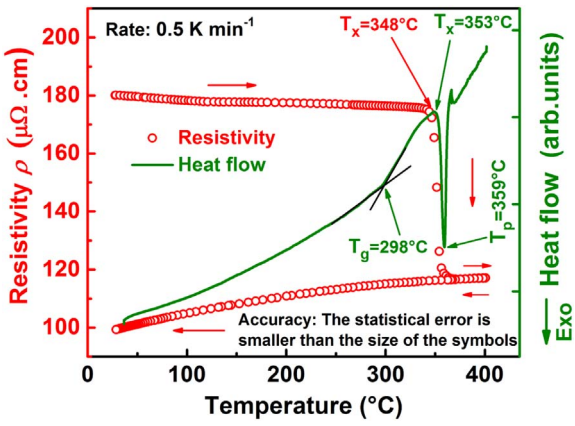

Fig. 8. The temperature dependence of the electrical resistivity (red squares left scale) and DSC trace (green curve right scale) of $Ni_{33.3}Zr_{66.7}$ metallic glass at heating rate of 0.5 K min^{-1}. The characteristic temperatures T_g (glass transition temperature), T_x (onset of the crystallization temperature), and T_p (peak temperature) are indicated. (For interpretation of the references to colour in this figure legend, the reader is referred to the web version of this article.)

measured. If it is measured, we can use the exact formula.

Temperature dependences of the electronic thermal conductivity, k_{el}, of $Ni_{33.3}Zr_{66.7}$ metallic glass calculated from the experimental data are presented in Fig. 7. The electronic thermal conductivity value of the glassy sample at room temperature is about 4.09 W m^{-1} K^{-1}, as shown in Fig. 7. The electronic thermal conductivity increases almost linearly with increasing temperature up to the onset of crystallization temperature with a positive temperature coefficient (PTC), then we observe a sudden rise, giving a larger value of 14.08 W m^{-1} K^{-1} at 400 °C. At cooling the electronic thermal conductivity decreases quasi-linearly down to room temperature. The room-temperature electronic thermal conductivity, k_{el}, of the crystallized ribbon is equals to 7.44 W m^{-1} K^{-1}. Thereby, the thermal conductivity value of the glassy state is lower than that of the crystalline state at room temperature. We observe no change of slope since the W.F. law contains a contribution proportional to T.

The calculated electronic contribution (k_{el}) for the $Ni_{33.3}Zr_{66.7}$metallic glass (at room temperature) is in good agreement with the results of $Zr_{55}Al_{10}Ni_5Cu_{30}$ BMGs and comparable to that of the $Pd_{40}Cu_{40-x}Cu_xP_{20}$ BMGs [44]. Moreover, Umetsu et al. [45] reported that the phonon conductivity, k_{Ph}, of Zr-based BMG in both glassy and crystallized state, is approximately constant, and presents a minor contribution (< 10%) to the total thermal conductivity, k_{total}, compared to the dominant contribution of k_{el}.

3.1.4. DSC measurements

In order to compare the results of resistivity measurements with calorimetric measurements, differential scanning calorimetry (DSC) was carried out at the same heating rate of 0.5 K min^{-1}. Both resistivity and DSC scans are presented together in Fig.8. The crystallization temperatures (T_x) obtained from the slope changes of the electrical resistivity and the Seebeck coefficient are in good agreement, whereas the crystallization onset temperature revealed by DSC analysis is shifted by 5 °C towards higher temperatures(see Fig. 8). This shift is explained by the immediate reaction of the resistivity to the electrons released at the detection of the phase transition, whereas in DSC measurements, the heat flux takes a longer time to react. Similar results have been observed in the literature [46,47]. In addition, the only exothermic peak observed by DSC analysis implies that the crystallization transition mechanism exhibits only one main process, this confirms the high purity of the studied alloy, which has low oxygen contamination during its ultrafast liquid quenching [48].

The heat flow curve of $Ni_{33.3}Zr_{66.7}$ metallic glass reveals that the glass transition temperature (T_g), and the onset crystallization temperature (T_x) are respectively identified as 298 °C and 353 °C, their difference giving rise to a large supercooled liquid region $\Delta T_x = T_x - T_g = 55$ °C. The crystallization onset temperature T_x (= 353 °C) is generally related to the nucleation process where the crystals begin to precipitate in the amorphous matrix, whereas, the peak temperature T_p (= 360 °C) (indicate the maximum temperature value of exothermic curve) corresponds to the growth mechanism [49]. During the crystallization process, the nucleation mechanism requires a greater quantity of energy than that of grain growth process [2]. The large SLR (= 55 °C) is mainly due to the difficulty of precipitation of the crystalline phase because of the high solid-liquid interfacial energy necessary for the transition from the disordered to the ordered state [50]. This may confirm that the $Ni_{33.3}Zr_{66.7}$MG exhibit a high thermal stability, which in turn indicates the high glass-forming ability. The crystallization temperature zone of $Ni_{33.3}Zr_{66.7}$ metallic glass indicated by the various measurement techniques (resistivity, ATP, and DSC) is almost similar.

3.2. Phase change at constant temperature

The isothermal experiments were carried out by heating the glassy ribbons at a constant rate of 0.5 K min^{-1} from room temperature up to 30 K below the annealing temperature, located above T_g and below T_x, in the supercooled liquid region (SLR) obtained from ATP and DSC experiments. Then the heating rate was gradually decreased to 0.1 Kmin^{-1} to the beginning of the isothermal test (at constant temperature of 335 °C)·The sample was maintained at this temperature for a certain period until the end of the crystallization process. Then rapid cooling to room temperature is used to keep the crystallized state of the heated samples.

Time-dependent isothermal measurements of both electrical resistivity and absolute thermoelectric power of $Ni_{33.3}Zr_{66.7}$ metallic glass were plotted at a constant temperature of 335 °C, during 240 min as shown in Fig. 9. The exponential decay of the resistivity starts from 175.7 μΩ cm and stabilizes at 109.7 μΩ cm. The time constant can be easily determined. The same pattern is observed on the ATP curve, which shows a strong decrease from an initial value of 3.05 μV K^{-1}. After 240 min, the ATP curve stabilizes at a value of 0.84 μV K^{-1} indicating the complete transformation of the amorphous phase to the crystalline phase. Since it is absolutely necessary to ensure a very well stabilized temperature during the isothermal experiments, the furnace temperature is also plotted as function of time throughout the experiment, as illustrated in Fig. 9. It can be seen that the temperature remain very stable around 335.47 ± 0.3 °C during the experiment time, which confirms the high thermal stability of the measuring system.

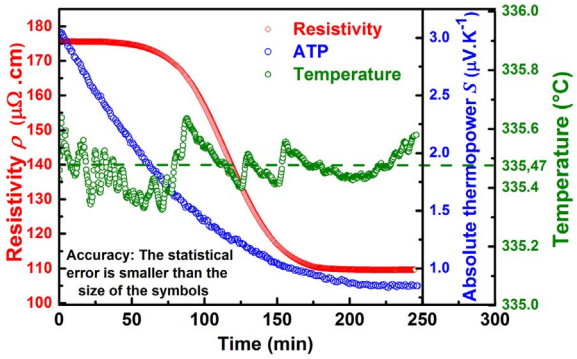

Fig. 9. Time dependent electrical resistivity (left scale) and ATP (right scale) during phase transformation of the $Ni_{33.3}Zr_{66.7}$ amorphous ribbons at the constant temperature of335 °C. The temperature stability at 335 °C during phase transformation is also plotted. It oscillates between 335.3 and 335.6 °C.

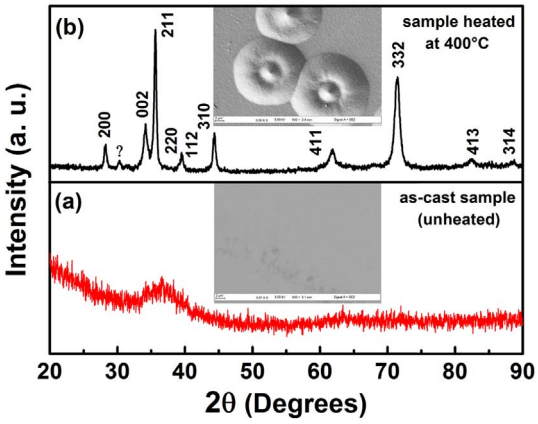

Fig. 10. X-ray diffraction pattern and SEM observation of $Ni_{33.3}Zr_{66.7}$ melt-spun ribbon, (a) in as-received condition (bottom), (b) after heating up to 400 °C (top) (heating rate of 0,5 K min^{-1}).

3.3. SEM and XRD analysis

Fig. 10(a) illustrates an XRD diffraction pattern of as-cast $Ni_{33.3}Zr_{66.7}$ MG. The XRD pattern mainly consisting of a single broad symmetric peak at about 37°, without any sharp Bragg diffraction peaks, characteristic for crystalline phases. This confirms the formation of a single glassy phase (amorphous nature) of $Ni_{33.3}Zr_{66.7}$ alloys. This fully amorphous structure is also confirmed by scanning electron microscopy (SEM) shown in the inset of Fig. 10(a), where no precipitate was observed on the ribbon surface. As shown in Fig. 10(b), the diffraction pattern of the preheated ribbon (i. e. annealed in isochronous regime up to 400 °C) contain the Bragg reflection peaks, indicating devitrification of the $Ni_{33.3}Zr_{66.7}$ glassy alloy. The SEM images of the crystallized glass revealed that the mean grain size is about 10 μm, as seen in the inset of Fig. 10(b).

The transition from the amorphous to the crystalline state is partially achieved after 33% of volume fraction transformed, during 80 min of isothermal heating at 335 °C, as shown in Fig. 11(a). Obviously, the inset of Fig. 11(a) shows the appearance (precipitation) of small micro-sized crystallites (of about 2 μm) in the residual matrix, which is also confirmed by the low-intensity peaks in the corresponding X-ray diffraction as shown in Fig. 11(b). By increasing the isothermal annealing time to 240 min, the diffraction peaks intensities become much more intense as shown in Fig. 11(b). The grain size of the crystallized phase is increased up to 10 μm (see inset of Fig. 11(b)), almost similar to that of the isochronous regime (up to 400 °C)·The time and temperature-dependent changes in the structural properties of $Ni_{33.3}Zr_{66.7}$ glass alloy indicate that the crystallized phase increases

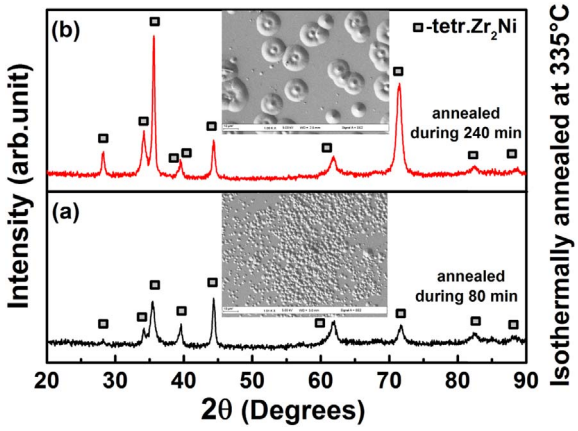

Fig. 11. X-ray diffraction pattern and SEM observation of isothermally annealed $Ni_{33.3}Zr_{66.7}$ MG at 335 °C, (a) after annealing for 80 min (bottom), (b) after annealing for 240 min (top).

under the effect of temperature and time.

The XRD diffraction patterns of the crystallized alloys indicates that the crystallized phase corresponds predominantly to $NiZr_2$ of tetragonal structure with the space group I4/mcm and having a crystal lattice parameter of a = 6.492 Å, c = 5.287 Å, and vol = 222.826 $Å^3$, in good agreement to reference 00-019-0857 from the ICDD-PDF2 2003 database. The sharp decrease in the electrical resistivity of the $Ni_{33.3}Zr_{66.7}$ amorphous alloy during the phase transition (crystallization) is also due to the appearance of the tetragonal $NiZr_2$ crystal structure embedded in the amorphous matrix. Grains of spherical geometry and a size of a few μm may change the band structure by changing the atomic arrangements of our alloy. Therefore, the appearance of this crystalline phase will favor the mobility of the electrons during the growth of the crystals, and thus gradually reduce the electrical resistivity until the end of the crystallization process [51]. Hence, the change of structure leads to a significant modification of the electronic transport properties.

4. Conclusions

In this study, we have investigated the electron transport behavior and thermal stability of the $Ni_{33.3}Zr_{66.7}$ metallic glass using simultaneous measurements of resistivity and absolute thermoelectric power (new methodology) with a very high degree of accuracy between room temperature and 400 °C. These characterization techniques are as an additional means of analysis equivalent to the DSC (if not better). The main results may be summarized as follows:

1. The room-temperature resistivity value of $Ni_{33.3}Zr_{66.7}$ metallic glass is equal to180.13 μΩ cm. By heating up to 330 °C, the $Ni_{33.3}Zr_{66.7}$ MG generates a negative TCR of the order of -1.17×10^{-10} Ω m K^{-1}, and then changes its sign after complete crystallization below 400 °C. This behavior is reproduced during the first cooling and then during the subsequent heating and cooling cycles. The amorphous to crystalline transformation has lowered the value of the resistivity of about 37%.
2. The Curie point is traduced by a change of resistivity slope at 120 °C.
3. The ATP value of $Ni_{33.3}Zr_{66.7}$ metallic glassy alloy measured at room temperature is positive (1.95 μV K^{-1}) and decreases to about 0.84 μV K^{-1} at 400 °C. Upon cooling, the absolute thermoelectric power of crystallized $Ni_{33.3}Zr_{66.7}$ glass reaches the value of 1.94 μV K^{-1} at room temperature, which is practically the same as that of the as-prepared, unheated glassy ribbon.
4. A local minimum detected on thermopower temperature dependence at about 155 °C by using a K-type thermocouple is related to the K-type thermocouple polynomials and Gaussian functions obtained from NIST's thermocouple tables. These polynomial and

Gaussian functions do not correspond to thermocouples that can be bought. The Roberts copper ATP measurements, taken as a reference, were used to validate the correction. Thus, it may be considered that our results fit excellently the Roberts values ($\sim 0.1\ \mu V\ K^{-1}$).

5. A wide supercooled liquid region $\Delta T_x = 55\ ^\circ C$ indicates a good thermal stability and high GFA of the $Ni_{33.3}Zr_{66.7}$ amorphous alloy. The additional characterization study of the $Ni_{33.3}Zr_{66.7}$ MGs using DSC and XRD confirms the thermal profile obtained by the resistivity and thermoelectric power measurements.
6. The isochronal and isothermal heat treatment of $Ni_{33.3}Zr_{66.7}$ metallic glass leads to the devitrification of the amorphous ribbon with tetragonal $NiZr_2$ crystallization product.
7. The high-accuracy of our ATP measurements allowed us to detect the glass transition temperature T_g, which is in good agreement with DSC measurements.

References

[1] S.Y. Luo, J.H. Li, J.B. Liu, B.X. Liu, Atomic modeling to design favored compositions for the ternary Ni-Nb-Zr metallic glass formation, Acta Mater. 76 (2014) 482–492 https://doi.org/10.1016/j.actamat.2014.06.003.

[2] A.H. Taghvaei, J. Eckert, A comparative study on the isochronal and isothermal crystallization kinetics of $Co_{46.45}Fe_{25.55}Ta_8B_{20}$ soft magnetic metallic glass with high thermal stability, J. Alloys Compd. 675 (2016) 223–230, http://dx.doi.org/10.1016/j.jallcom.2016.03.053.

[3] C. Peng, Z.H. Chen, X.Y. Zhao, A.L. Zhang, L.K. Zhang, D. Chen, Crystallization kinetics of $Zr_{60}Cu_{25}Fe_5Al_{10}$ bulk metallic glass, J. Non-Cryst. Solids 405 (2014) 7–11 (doi:10.1016/j.jnoncrysol.2014.08.030).

[4] R.M. Khusnutdinoff, Local structural features of metallic alloys: $Ni_{33}Zr_{67}$ and $Ni_{50}Zr_{50}$, Acta Phys. Pol. A 129 (3) (2016) 3–6 (http://dx.doi.org/10.12693/APhysPolA.129.293).

[5] I. Kaban, P. Jóvári, V. Kokotin, O. Shuleshova, B. Beuneu, K. Saksl, N. Mattern, J. Eckert, A.L. Greer, Local atomic arrangements and their topology in Ni-Zr and Cu-Zr glassy and crystalline alloys, Acta Mater. 61 (7) (2013) 2509–2520, http://dx.doi.org/10.1016/j.actamat.2013.01.027.

[6] D. Bhattacharya, T.V. Chandrasekhar Rao, K.G. Bhushan, K. Ali, A. Debnath, S. Singh, A. Arya, S. Bhattacharya, S. Basu, Thermal evolution of nanocrystalline co-sputtered Ni-Zr alloy films: structural, magnetic and MD simulation studies, J. Alloys Compd. 649 (2015) 746–754, http://dx.doi.org/10.1016/j.jallcom.2015.07.220.

[7] F. Orbanić, I. Kokanović, Impact of quenched disorder and crystallization on electrical resistivity in $Zr_{67}Co_{33}$ metallic glass, J. Non-Cryst. Solids 428 (2015) 31–35 (doi:10.1016/j.jnoncrysol.2015.07.046).

[8] I. Kokanović, The magnetic susceptibility of hydrogen-doped partially crystalline $(Zr_{76}Ni_{24})_{1-x}H_x$ metallic glasses, J. Magn. Magn. Mater. 321 (13) (2009) 1985–1989, http://dx.doi.org/10.1016/j.jmmm.2008.12.031.

[9] B. Liu, N. Zuo, F. Ye, Abnormal change of electrical resistivity in the $Cu_{46}Zr_{46}Al_8$ bulk metallic glass during crystallization, Mater. Lett. 171 (2016) 285–288, http://dx.doi.org/10.1016/j.matlet.2016.02.117.

[10] K. Khalouk, Etude du transport électronique de métaux liquides, amorphes et cristallins à hautes températures, PhD. thesis Paul Verlaine Université Metz, 2009.

[11] A. Makradi, J.G. Gasser, S. Belouettar, Electronic transport properties of liquid zinc and zinc- germanium alloys: theory versus experiment, J. Non-Cryst. Solids 356 (6–8) (2010) 400–406 (doi:10.1016/j.jnoncrysol.2009.11.027).

[12] A.B. Abdellah, B. Grosdidier, S.M. Osman, S.M. Mujibur Rahman, M. Mayoufi, J. Ataati, J.G. Gasser, Spin-state dependence of electrical resistivity and thermoelectric power of molten Al-Mn alloys: experiment and theory, J. Alloys Compd. 658 (2016) 1010–1019, http://dx.doi.org/10.1016/j.jallcom.2015.10.271.

[13] L. Abadlia, Etude des propriétés de transport électroniques des matériaux métalliques amorphes, PhD thesis University Badji Mokhtar of Annaba, 2015.

[14] F. Gasser, Mesures automatisées de la résistivité et du pouvoir thermoélectrique absolu (Automatic measurement of resistivity and absolute thermoelectric power), Software registered at the Agency for the Protection of Programs, 10 May 2010 (Reg. No. FR.001.190009.000.S.P.2010.000.31235).

[15] J.G. Gasser, K. Khalouk, F. Gasser, Procédé et appareils de mesure du pouvoir thermoélectrique absolu d'un échantillon (Process and equipment for absolute thermoelectric power measurement), Patent FR1257261, Institut National de la Protection Industrielle (INPI), July 2012, p. 26.

[16] A. Bath, Contribution a l'étude des propriétés de transport électronique d'alliages métalliques liquides (Cd-Zn, Zn-Sb, Cd-Sb) en relation avec les effets d'ordre structuraux, University of Metz, PhD. thesis, 1983.

[17] R.B. Roberts, F. Righini, R.C. Compton, Philos. Mag. B 52 (6) (1985) 1147–1163 (doi:10.1080/13642818508238957).

[18] L. Abadlia, F. Gasser, K. Khalouk, M. Mayoufi, J.G. Gasser, New experimental methodology, setup and LabView program for accurate absolute thermoelectric power and electrical resistivity measurements between 25 and 1600 K: application to pure copper, platinum, tungsten, and nickel at very high temperatures new experimental methodology, setup and LabView program for accurate absolute thermoelectric power and electrical resistivity measurements between 25 and 1600 K: application to pure copper, platinum, tungsten, and nickel at very high temperatures, Rev. Sci. Instrum. 85 (2014) 095121 https://doi.org/10.1063/1.4896046.

[19] Z.J. Ma, Y.C. Guo, L.T. Li, P.H. Gao, Z. Yang, X.R. Zeng, The effect of cooling rate on the plasticity of amorphous metal, J. Alloys Compd. 648 (2016) 18–21 (doi:10.1016/j.jallcom.2015.06.212).

[20] M. Deanko, M. Paluga, D.M. Kepaptsoglou, D. Muller, P. Mrafko, D.D. Janičkovič, E. Christoforou, I. Skorvánek, P. Švec, Pecularities of electrical resistivity during transformations in amorphous and nanocrystalline alloys, J. Alloys Compd. 435 (2007) 248–251 (doi:10.1016/j.jallcom.2006.08.124).

[21] K. Rhie, D.G. Naugle, A.K. Bhatnagar, The Hall effect in amorphous $(Zr_{0.64}Ni_{0.36})_{1-x}M_x$ alloys (M = Al, Ga), Z, Phys.B-Condensed Matter. 416 (3) (1990) 411–416, http://dx.doi.org/10.1007/BF01313322.

[22] E. Babić, R. Ristić, M. Miljak, M.G. Scott, G. Gregan, Superconductivity in zirconium-nickel glasses, Solid State Commun. 39 (1) (1981) 139–141, http://dx.doi.org/10.1016/0038-1098(81)91064-4.

[23] Y. Yamada, Y. Itoh, T. Matsuda, U. Mizutani, Electron transport studies of $Ni_{33}Zr_{67}$-based metallic glasses containing H, B, Al and Si, J. Phys. F: Met. Phys. 17 (1987) 2313–2322, http://dx.doi.org/10.1088/0305-4608/17/11/020.

[24] Z. Altounian, C.L. Foiles, B. Muir, J.O. Strom-Olsen, Thermoelectric power of Ni-Zr metal glasses, Phys. Rev. B 27 (4) (1983) 1955, http://dx.doi.org/10.1103/PhysRevB.27.1955.

[25] J.H. Mooij, Electrical conduction in concentrated disordered transition metal alloys, Phys. Stat. Sol. A. 17 (1973) 521–530, http://dx.doi.org/10.1002/pssa.2210170217.

[26] H.W. Yang, J. Gong, R.D. Li, J.Q. Wang, Thermal variation of electrical resistance of an $Al_{85}Ni_5Y_8Co_2$ metallic glass free of quenched-in nuclei, J. Non-Cryst. Solids 355 (2009) 2205–2208 (doi:10.1016/j.jnoncrysol.2009.08.001).

[27] I. Kaban, K. Khalouk, F. Gasser, J.G. Gasser, J. Bednarčik, O. Shuleshova, I. Okulov, T. Gemming, N. Mattern, J. Eckert, In situ studies of temperature-dependent behaviour and crystallization of $Ni_{36.5}Pd_{36.5}P_{27}$ metallic glass, J. Alloys Compd. 615 (2014) S208–S212 (doi:10.1016/j.jallcom.2013.12.259).

[28] Frédéric Sar, Souad Mhiaoui, Jean-Georges Gasser, Thermal conductivity of liquid lead–bismuth alloys, possible coolants for fourth generation spallation nuclear reactors, J. Non-Cryst. Solids 353 (2007) 3622–3627, http://dx.doi.org/10.1016/j.jnoncrysol.2007.05.171.

[29] E. Gratz, The influence of magnetism on transport properties (electrical resistivity, thermopower and thermal conductivity) in rare earth compounds, Phys. Scr. T1 (1982) 97–99, http://dx.doi.org/10.1088/0031-8949/1982/T1/030.

[30] K. Shirakawa, S. Ohnuma, M. Nose, T. Masumoto, Invar characteristics of amorphous (Fe, Co and Ni)-Zr alloys, IEEE Trans. Magn. 16 (5) (1980) 910–912, http://dx.doi.org/10.1109/TMAG.1980.1060737.

[31] B. Liu, N. Zuo, F. Ye, Abnormal change of electrical resistivity in the $Cu_{46}Zr_{46}Al_8$ bulk metallic glass during crystallization, Mater. Lett. 171 (2016) 285–288, http://dx.doi.org/10.1016/j.matlet.2016.02.117.

[32] B. Liu, F. Ye, Low temperature heat capacity and electrical resistivity of the $Ti_{40}Zr_{25}Cu_{12}Ni_3Be_{20}$ glass forming alloy, Intermetallics 75 (2016) 31–36, http://dx.doi.org/10.1016/j.intermet.2016.05.010.

[33] J. Antonowicz, P. Jaśkiewicz, L. Nowiński, K. Pękała, Analysis of nanocrystallization process of amorphous $Al_{90}Y_{10}$ alloy, J. Non-Cryst. Solids 329 (2003) 77–81, http://dx.doi.org/10.1016/j.jnoncrysol.2003.08.016.

[34] A.J. Kailath, K. Dutta, T.C. Alex, A. Mitra, Crystallization study of $Cu_{56}Zr_7Ti_{37}$ metallic glass by electrical resistivity measurement, J. Mater. Sci. Technol. 27 (3) (2011) 275–279, http://dx.doi.org/10.1016/S1005-0302(11)60062-5.

[35] J.M. Ziman, A theory of the electrical properties of liquid metals. I: the monovalent metals, Philos. Mag. 6 (68) (1961) 1013–1034, http://dx.doi.org/10.1080/14786436108243361.

[36] K. Pękała, R. Trykozko, Thermoelectric power of amorphous alloys Ni_xZr_{1-x}, J, Phys. Lett. A 86 (3) (1981) 176–178 (doi:10.1016/0375-9601(81)90861-6).

[37] A.K. Bhatnagar, R. Pan, D.G. Naugle, Electron transport properties of amorphous $(Zr_{0.64}Ni_{0.36})_{1-x}Al_x$ alloys, Phys. Rev. B 39 (17) (1989) 12460, , http://dx.doi.org/10.1103/PhysRevB.39.12460.

[38] K. Pękała, D. Oleszak, Electron transport properties of amorphous alloys $Ni_{59}Zr_{20}Ti_{16}M_5$ (M = Nb, Si), Rev. Adv. Mater. Sci. 18 (2008) 197–201.

[39] Y.K. Kuo, K.M. Sivakumar, C.A. Su, C.N. Ku, S.T. Lin, A.B. Kaiser, J.B. Qiang, Q. Wang, C. Dong, Measurement of low-temperature transport properties of Cu-based Cu-Zr-Ti bulk metallic glass, Phys. Rev. B 74 (1) (2006) 014208, , http://dx.doi.org/10.1103/PhysRevB.74.014208.

[40] K. Pękała, J. Antonowicz, P. Jaskiewicz, T. Drobiazg, J. Konupek, Influence of quasicrystalline phase on transport processes in$Zr_{70}Pd_{30}$ amorphous alloy, J. Alloys Compd. 500 (2010) 145–148, http://dx.doi.org/10.1016/j.jallcom.2010.03.243.

[41] R.B. Roberts, The absolute scale of thermoelectricity II, Philos. Mag. B 43 (6) (1981) 1125–1135, http://dx.doi.org/10.1080/01418638108222579.

[42] P.G. Klemens, R.K. Williams, Thermal conductivity of metals and alloys, Int. Met. Rev. 31 (1) (1986) 197–215, http://dx.doi.org/10.1179/imtr.1986.31.1.197.

[43] K. Khalouk, M. Mayoufi, J.G. Gasser, Are there phase transitions in liquid metallic alloys? Philos. Mag. 90 (20) (2012) 2695–2709, http://dx.doi.org/10.1080/14786431003745310.

[44] M. Yamasaki, S. Kagao, Y. Kawamura, Thermal diffusivity and conductivity of $Zr_{55}Al_{10}Ni_5Cu_{30}$ bulk metallic glass, Scr. Mater. 53 (1) (2005) 63–67, http://dx.doi.org/10.1016/j.scriptamat.2005.03.021.

[45] R.Y. Umetsu, R. Tu, T. Goto, Thermal and electrical transport properties of Zr-based bulk metallic glassy alloys with high glass-forming ability, Mater. Trans. 53 (10) (2012) 1721–1725, http://dx.doi.org/10.2320/matertrans.M2012163.

[46] A.K. Panda, I. Chattoraj, A. Mitra, Crystallization and magnetic properties of rapidly solidified Fe-Nb-M-Si-B (M = Cu,Mn, Pt), Mater. Sci. Eng. A 304–306 (2001) 950–953, http://dx.doi.org/10.1016/S0921-5093(00)01603-8.

[47] A.K. Panda, S. GhoshChowdhury, A. Mitra, N. Nishiyama, A. Inoue, Electron transport behaviour and soft magnetic properties of bulk amorphous $Fe_{72}Si_4B_{20}Nb_4$ alloy, J. Phys. D. Appl. Phys. 39 (16) (2006) 3536–3542, http://dx.doi.org/10.1088/0022-3727/39/16/003.

[48] S. Boutet, G. Steele, M. Dikeakos, Z. Altounian, Influence of oxygen impurities on the crystallization mechanism of $NiZr_2$ metallic glasses, J. Appl. Phys. 89 (4) (2001) 2441–2446, http://dx.doi.org/10.1063/1.1334920.

[49] F.X. Qin, H.F. Zhang, B.Z. Ding, Z.Q. Hu, Nanocrystallization kinetics of Ni-based bulk amorphous alloy, Intermetallics 12 (10) (2004) 1197–1203 (doi:10.1016/j.intermet.2004.04.015).

[50] J.S.C. Jang, S.F. Tsao, L.J. Chang, G.J. Chen, J.C. Huang, Crystallization kinetics of the $Zr_{61}Al_{7.5}Cu_{17.5}Ni_{10}Si_4$ alloy using isothermal DSC and TEM observation, J. Non-Cryst. Solids 352 (2006) 71–77, http://dx.doi.org/10.1016/j.jnoncrysol.2005.11.004.

[51] I. Kokanovic, Influence of hydrogen doping on the electrical resistivity of partially crystalline, J. Alloys Compd. 481 (2009) 22–27 (doi:10.1016/j.jallcom.2009.03.040).